SEMI-ANALYTICAL ESTIMATION OF THE PROBABILITY OF CAPTURE INTO 1:1 GROUND-TRACK RESONANCE OF A LOW-THRUST SPACECRAFT AROUND AN ASTEROID.

Wail Boumchita[(1)], **Jinglang Feng**[(1)], **Anatoly Neishtadt**[(2)]

[(1)]*University of Strathclyde, G1 1XJ Glasgow, UK , (wail.boumchita,jinglang.feng)@strath.ac.uk*
[(2)]*Loughborough University, LE11 3TU Loughborough, UK , a.neishtadt@lboro.ac.uk*

ABSTRACT

This paper presents a semi-analytical methodology to estimate the probability of capture into 1:1 ground-track resonance of a low-thrust spacecraft around an asteroid. The system dynamics are described by a Hamiltonian model that considers the perturbations from the irregular gravitational field up to the second order and degree, and the continuous low thrust that remains constant in magnitude and is always in the direction opposite to the spacecraft's velocity. The model focuses on the equatorial case of the 1:1 ground-track resonance. When a trajectory is close to the resonance location, its behavior becomes non-deterministic, making it necessary to estimate the probability of capture into resonance. A fourth-order polynomial is used to numerically approximate the separatrices of the resonance region, while the change of the system's energy balance when the trajectory crosses the separatrices is determined with a global adaptive quadrature method. Subsequently, the probability of capture into resonance is estimated, and the accuracy of the results is verified by comparing them to numerical simulations based on the perturbed Hamilton's equations of motion. This research makes a significant contribution to the field of astrodynamics by systematically and efficiently analyzing the probability of low-thrust spacecraft capture into ground-track resonance around asteroids.

1 INTRODUCTION

In 2011, the DAWN spacecraft successfully arrived at the asteroid Vesta. During the approach phase, the spacecraft descended from a high-altitude mission orbit (HAMO) to a low-altitude mission orbit (LAMO) utilizing low-thrust propulsion. The orbital radii of the HAMO and LAMO are 1000 km and 460 km, respectively [1]. However, the use of low-thrust propulsion during the descent phase posed a risk of capturing the spacecraft into ground-track resonance (GTR) around Vesta, caused by the chaotic layer surrounding the resonance region [2]. This is a type of resonance in which the period of revolution of the spacecraft is commensurable to the period of rotation of the asteroid around its axis. An example of 1:1 GTR is the geostationary orbit, in which the period of revolution of the spacecraft is equal to the period of rotation of the Earth around its spin axis [3]. This mission demonstrated the possibility of relying on low-thrust propulsion for the majority of the mission duration [4] [5]. The use of low-thrust propulsion allows for more efficient use of fuel and longer mission duration but also poses some challenges in terms of trajectory design [6]. However, the motion around Vesta is more complex due to its irregular gravitational field. The spacecraft at each revolution encounters the same gravitational configuration, the effect of which accumulates and significantly changes the orbit eccentricity and inclination [7]. The capture of a spacecraft into a GTR has the potential to significantly impact the success of a mission by preventing the reach of lower altitudes and the achievement of

scientific objectives.

The primary aim of this paper is to utilize the Hamiltonian formalism to analyze the capture into GTR phenomena and estimate the probability of capture into 1:1 GTR through a semi-analytical approach. The methodology is based on analyzing the energy change that occurs when the spacecraft enters into resonance with Vesta. a two-degree-of-freedom Hamiltonian model associated with the 1:1 GTR in the equatorial case. This includes the perturbations from the irregular gravitational field up to the second order, along with continuous low thrust that remains constant in magnitude and is always in the direction opposite to the spacecraft's velocity. Through this process, the equilibrium points, as well as the libration and circulation regions, are identified. A global adaptive quadrature method is employed to evaluate the system's energy balance as the trajectory crosses the separatrix. Then, the probability of capture into resonance is estimated as a function of the energy balance, and the accuracy of the results is verified by comparing them with numerical simulations based on the equations of motion derived from the Hamiltonian. A significant advantage of a semi-analytical investigation is the ease with which the results can be obtained when the data changes. Our approach is highly adaptable to similar missions, as the numerical values of parameters such as the shape and mass of the asteroid or spacecraft orbit may vary, but the methodology remains the same, and the results can be readily adapted accordingly.

The paper is organized as follows: Section 2 discusses the characterization of the dynamical environment around Vesta and the identification of the dominant perturbations. Section 3 provides a description of the dynamic model for the motion of Dawn around Vesta and derives the equations of motion. The semi-analytical methodology used to estimate the probability of capture into 1:1 GTR is presented in Section 4. The results of the semi-analytical estimation and the comparison with numerical estimations are discussed in Section 5, where the errors are also characterized. Finally, Section 6 summarizes the paper and presents the conclusions.

2 MAIN PERTURBATIONS

The physical parameters of Vesta are listed in Table 1, and it is assumed to rotate uniformly around a constant direction in inertial space. The unnormalized Stokes coefficients of Vesta are given in [8].

Table 1: Vesta's physical parameters [1]

Gravitational constant	μ	17.5 km^3/s^2
Reference radius	R_e	300 km
Angular velocity	ω	3.2671×10^{-4} rad/s

The spacecraft is subject to the following perturbations [9]:

- Vesta's gravitational perturbations

$$a_{nm} = (n+1)\frac{\mu}{r^2}\frac{R_e^n}{r^n}\sqrt{C_{nm} + S_{nm}}, \tag{1}$$

- Sun's gravitational perturbation

$$a_{Sun} = \frac{2\mu_{Sun}}{d_{Sun}^3}r, \tag{2}$$

- solar radiation pressure perturbation

$$a_{SRP} = C_r \frac{A}{m} P_\odot \tag{3}$$

where r represents the distance from the spacecraft to Vesta, C_{nm} and S_{nm} are the unnormalized Stokes coefficients, n and m are the degree and order of the spherical harmonic expansion considered, $\mu_\odot$ represents the gravitational constant of the Sun, $d_\odot$ is the distance of the spacecraft from the Sun, $C_r = 0.25$ is the reflectivity coefficient of the spacecraft, $A/m = 0.04$ is the area-to-mass ratio of the spacecraft, and $P_\odot$ is the solar radiation pressure at a distance $d_\odot$ from the Sun. The magnitudes of the main perturbations at different orbital radii are illustrated in Fig.1. At the orbital radius corresponding
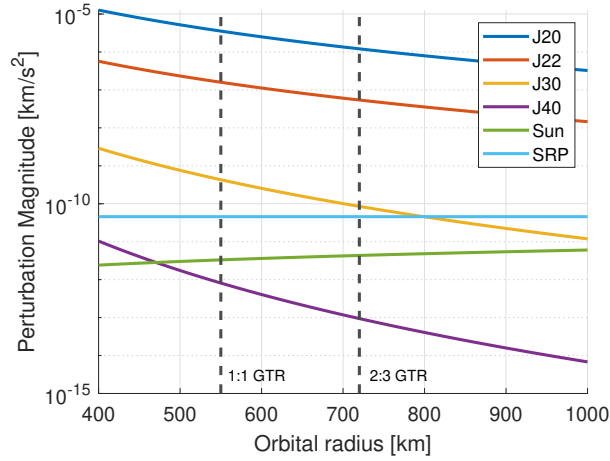

Figure 1: Order of magnitude of the various perturbations to which the DAWN spacecraft is subject at different orbital radii. The location of the 1:1 and 2:3 GTRs are highlighted for reference.

to the 1:1 GTR, i.e. 550 km, Vesta's gravitational perturbations are an order of magnitude stronger than the perturbations from the Sun's gravitational attraction, and the solar radiation pressure. This highlights the importance of accurately accounting for Vesta's gravitational influence in the dynamic modeling of the spacecraft's trajectory. Furthermore, it is worth noting that the relative magnitudes of these perturbations can vary significantly depending on the orbital radius of the spacecraft. Given the dominant effect of Vesta's irregular gravitational perturbations at the 1:1 GTR and the potential impact on the spacecraft's trajectory, in this paper, only these perturbations are considered in the dynamic model.

3 DYNAMIC MODEL

This section presents the Hamiltonian that governs the motion of a spacecraft around an asteroid with an irregular gravitational field. Specifically, the Hamiltonian is focused on the 1:1 GTR in the equatorial case and the resulting equations of motion are established. The impact of non-conservative forces, such as the low-thrust, is also accounted for. To simplify the model, it is expanded around the 1:1 GTR location, resulting in a pendulum-like expression.

3.1 Hamiltonian model

The gravitational potential of a central body can be represented as a function of spherical harmonics [10], where the shape and density variations of an asteroid are expressed using the Stokes coefficients. The potential, denoted as V, is expressed as a series expansion of spherical harmonics up to degree n and order m as

$$V = \frac{\mu}{r} + \sum_{n=2}^{\infty} \sum_{m=0}^{n} \sum_{p=0}^{n} \sum_{q=-\infty}^{\infty} \frac{\mu R_e^n}{a^{n+1}} F_{nmp}(i) G_{npq}(e) S_{nmpq}(\omega, M, \Omega, \theta), \tag{4}$$

where $F_{nmp}(i)$ and $G_{npq}(e)$ are functions of the inclination i and eccentricity e, respectively, a is the semi-major axis, ω is the argument of periapsis, M is the mean anomaly, Ω is the longitude of the ascending node, θ is the sidereal time and n, m, p, q are all integers and

$$S_{nmpq} = \begin{cases} C_{nm} \cos \Psi_{nmpq} + S_{nm} \sin \Psi_{nmpq}, & \text{if } n - m \text{ is even}, \\ -S_{nm} \cos \Psi_{nmpq} + C_{nm} \sin \Psi_{nmpq}, & \text{if } n - m \text{ is odd}, \end{cases} \tag{5}$$

where Ψ_{nmpq} is the Kaula's phase angle that is defined as

$$\Psi_{nmpq} = (n - 2p)\omega + (n - 2p + q)M + m(\Omega - \theta). \tag{6}$$

When the rate of change of Kaula's phase angle $\dot{\Psi}_{nmpq}$ is close to zero, the GTRs occur. Let $L = \sqrt{\mu a}$, the Hamiltonian describing the spacecraft's motion around an asteroid with an irregular gravitational field is defined as

$$\mathcal{H} = -\frac{\mu^2}{2L^2} + \sum_{n=2}^{\infty} \sum_{m=0}^{n} \sum_{p=0}^{n} \sum_{q=-\infty}^{\infty} R_e^n \frac{\mu^{n+2}}{L^{2n+2}} F_{nmp}(i) G_{npq}(e) S_{nmpq}(\omega, M, \Omega, \theta) + \dot{\theta} \Lambda, \tag{7}$$

where Λ is the conjugated momentum to the sidereal time θ and the term $\dot{\theta}\Lambda$ accounts for the asteroid's rotation. The gravitational term of second degree and order primarily affects the dynamics of the system close to the 1:1 GTR [11]. Therefore, the Hamiltonian used in the analysis considers only this harmonic. The Hamiltonian that describes the 1:1 GTR dynamics around the asteroid is expressed as

$$\mathcal{H}_{1:1} = -\frac{\mu^2}{2L^2} + R_e^2 \frac{\mu^4}{L^6} F_{220}(i) G_{200}(e) S_{2200}(\omega, M, \Omega, \theta) + \dot{\theta} \Lambda. \tag{8}$$

For an equatorial orbit ($i = 0°$), the Hamiltonian is

$$\mathcal{H}_{1:1} = -\frac{\mu^2}{2L^2} - \frac{15}{2} R_e^2 \frac{\mu^4}{L^6} \left(-\frac{3}{5} + \frac{G^2}{L^2} \right) C_{22} \cos(2(M + \omega - \theta)) + \dot{\theta} \Lambda, \tag{9}$$

where L and $G = L\sqrt{1 - e^2}$ are the momenta conjugated respectively to M and ω. A canonical transformation is performed with the generating function $F = (M + \omega - \theta)L' + (-\omega)G' + \theta\Lambda'$ which leads to the new set of canonical variables

$$\sigma = M + \omega - \vartheta \quad , \quad Q = -\omega \quad , \quad L = L' \quad , \quad G = L' - K \quad , \quad \Lambda = -L' + \Lambda'. \tag{10}$$

The new Hamiltonian $\tilde{\mathcal{H}}_{1:1}$ is

$$\tilde{\mathcal{H}}_{1:1} = -\frac{\mu^2}{2L^2} - \frac{15}{2}R_e^2\frac{\mu^4}{L^6}\left(-\frac{3}{5} + \frac{(L-G)^2}{L^2}\right)C_{22}\cos(2\sigma) - \dot{\theta}L, \tag{11}$$

where the prime sign is dropped for clarity. Fig.2 shows the phase portrait of $\tilde{\mathcal{H}}_{1:1}$, where the upper separatrices are indicated with the red line l_1 and the lower ones with l_2.
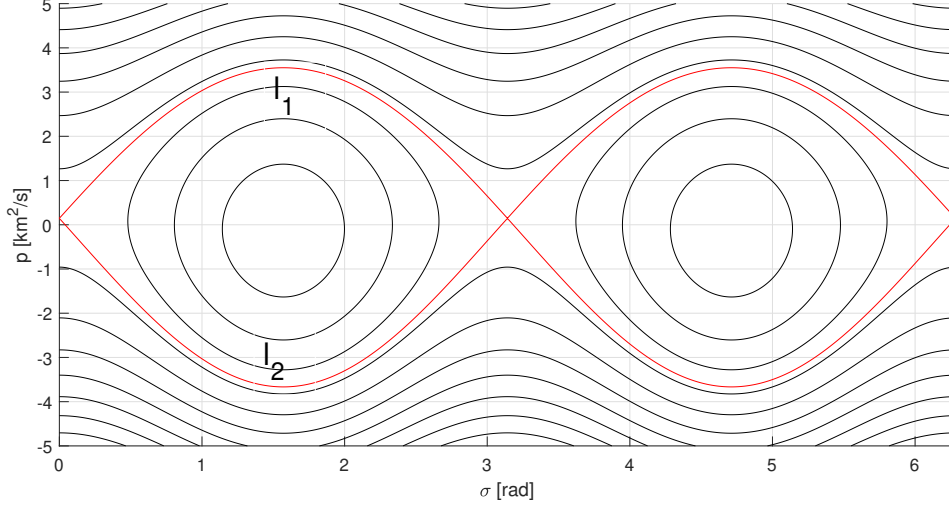

Figure 2: Phase portrait of $\tilde{\mathcal{H}}_{1:1}$. The red lines l_1 represent the upper separatrices, while l_2 represents the lower separatrices.

3.2 Non-conservative forces

One approach to account for energy dissipation is to add terms to Hamilton's equations of motion that account for the presence of dissipative forces [12]. The change of L over time can be related to the change of a as

$$\frac{dL}{dt} = \frac{\mu}{2L}\frac{da}{dt}. \tag{12}$$

From [13], the rate of change of the semi latus rectum $p = a(1-e^2)$ due to tangential accelerations is

$$\frac{dp}{dt} = \frac{2}{v}a_t p, \tag{13}$$

where v is the spacecraft velocity and at is the magnitude of the tangential acceleration from the low-thrust. So,

$$\frac{dL}{dt} = T_L = -\frac{T}{m}\frac{L^2}{\mu}. \tag{14}$$

Since $K = L - G$, the rate of change of K over time is

$$\frac{dK}{dt} = \frac{dL}{dt} - \frac{dG}{dt}. \tag{15}$$

The rate of change of G over time is related to the rate of change of e as

$$\frac{dG}{dt} = -\frac{T}{m}\frac{LG}{\mu} - e\frac{L^2}{G}\frac{de}{dt}. \tag{16}$$

From [13], the rate of change of e due to the low-thrust is

$$\frac{de}{dt} = \frac{1}{v}\left(-2\frac{T}{m}(e + \cos\theta)\right). \tag{17}$$

To eliminate the dependency on the true anomaly, the expression is averaged over the mean anomaly. Considering the second term of de/dt, the following integral is defined

$$I = \frac{1}{2\pi}\int_0^{2\pi} \cos\theta \, dM. \tag{18}$$

The integrand and the differential of the mean anomaly are expressed as a function of the eccentric anomaly E as

$$\cos\theta = \frac{\cos E - e}{1 - e\cos E} \quad \text{and} \quad dM = (1 - e\cos E)dE. \tag{19}$$

So the integral I becomes

$$I = \frac{1}{2\pi}\int_0^{2\pi}(\cos E - e)dE = -e. \tag{20}$$

Therefore, $de/dt = 0$. Finally, the rate of change of K is

$$\frac{dK}{dt} = T_K = -\frac{T}{m}\frac{LK}{\mu}. \tag{21}$$

Introducing the variable $p = L - Lr$, the equations of motion are

$$\begin{cases} \dot{\sigma} = \frac{d\tilde{\mathcal{H}}_{1:1}}{dp} \\ \dot{p} = -\frac{d\tilde{\mathcal{H}}_{1:1}}{d\sigma} + T_L \\ \dot{K} = T_K \end{cases} \tag{22}$$

Fig.3 shows the numerical verification of the resonance capture phenomenon for $e = 0.5$, with a set of uniformly distributed initial resonance angles between $[0,2\pi]$ and the initial altitude of 700 km. The simulation results indicate that the spacecraft is captured into resonance, as highlighted in red in Fig.3. Once captured, the momentum p exhibits libration around the resonance location at $p = 0$, as shown in the upper left plot of Fig.3. The upper right plot in Fig.3 shows the trajectory of the system in phase space, where the trajectory captured into resonance rotates around the stable equilibrium point $(\sigma,p) = (\pi/2,0)$. During the system's evolution, the momentum K decreases, and e remains almost constant until the separatrix crossing. After that, e starts to oscillate, and the average value decreases over time.
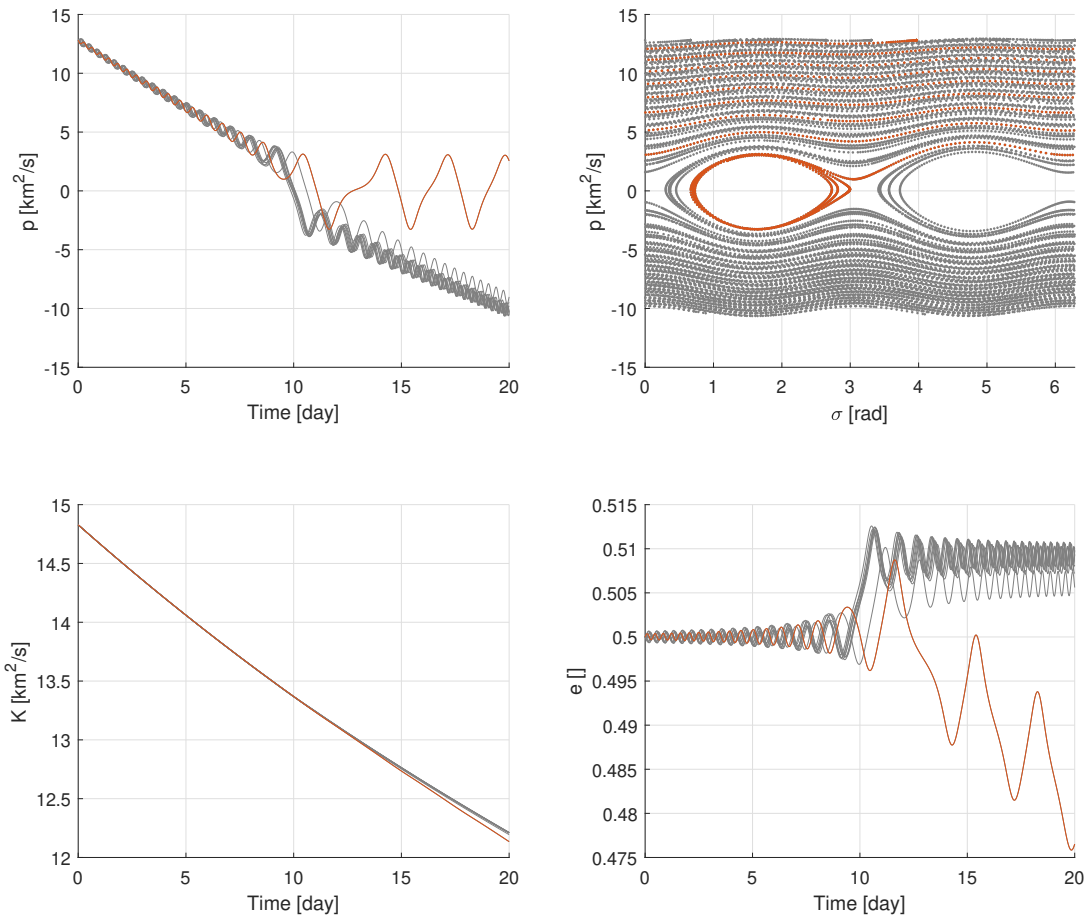
Figure 3: Evolution of p, K, and e over time and representation in phase space of the resonance crossing with $T = 20$ mN. The capture case is highlighted in red.

3.3 Pendulum approximation

In this section, an approximation of the complete Hamiltonian model is presented. Considering Eq.11, the Hamiltonian is divided as

$$\tilde{\mathcal{H}}_{1:1} = -\frac{\mu^2}{2L^2} - A(L, K)\cos(2\sigma) - \dot{\theta}L. \tag{23}$$

The resonance is located at L_r defined from

$$\frac{\mu^2}{L_r^3} = \dot{\theta}. \tag{24}$$

Then, the Hamiltonian is expanded around the resonance up to the second order leading to

$$\hat{\mathcal{H}}_{1:1} = -\frac{1}{2}\alpha p^2 - \hat{A}(L_r, K)\cos(2\sigma), \tag{25}$$

where

$$\hat{A}(L_r, K) = \frac{15}{2}R_e^2\frac{\mu^4}{L_r^6}\left(-\frac{3}{5} + \frac{(L_r - K)^2}{L_r^2}\right)C_{22} \quad \text{and} \quad \alpha = \frac{3\mu^2}{L_r^4}, \tag{26}$$

and the constant term is discarded. The Hamiltonian $\hat{\mathcal{H}}_{1:1}$ resembles the structure of a pendulum's Hamiltonian, composed of two main components: a quadratic term that represents the system's kinetic energy, and another term that accounts for the system's potential energy.

4 METHODOLOGY

This section presents the semi-analytical methodology to estimate the probability of capture into 1:1 GTR. The domain (σ, p) where the initial conditions are uniformly distributed is defined and denoted by U. A subset of initial conditions, labeled as U_{res}, can be identified within this domain, which corresponds to the capture of the system into the resonance domain. Then, the probability of capture into resonance can be determined by

$$Pr = \frac{\text{mes}U_{res}}{\text{mes}U}, \tag{27}$$

where $\text{mes}U_{res}$ and $\text{mes}U$ are the volumes of domains of U_{res} and U in phase space, respectively. This formulation is suitable only for numerical evaluation of the probability. To obtain an analytical estimation, it is necessary to express the probability in a different form using the energy-related quantities of the system. From [14], the probability of capture into 1:1 GTR is defined as

$$Pr = \frac{\int_{l_1 \cup l_2} d\tilde{\tilde{\mathcal{H}}}_{1:1}/dt\, d\tau}{\int_{l_1} d\tilde{\tilde{\mathcal{H}}}_{1:1}/dt\, d\tau}, \tag{28}$$

where $\tilde{\tilde{\mathcal{H}}}_{1:1} = \tilde{\mathcal{H}}_{1:1} - \tilde{\mathcal{H}}_{SP}$ and $\tilde{\mathcal{H}}_{SP}$ is the value of the Hamiltonian $\tilde{\mathcal{H}}_{1:1}$ at the saddle point. The integral in the numerator is computed along the upper separatrix l_1 and the lower separatrix l_2, whereas the integral in the denominator is calculated only along the upper separatrix. These integrals are improper as the motion along a separatrix takes an infinite amount of time. Thus, the normalization of the Hamiltonian guarantees the convergence of the integrals [15].

4.1 Complete model

The probability estimation is based on the normalized complete Hamiltonian model $\tilde{\bar{\mathcal{H}}}_{1:1}$. The saddle points are defined from

$$\frac{\partial \tilde{\bar{\mathcal{H}}}_{1:1}}{\partial p} = 0 \quad \text{and} \quad \sigma = 0, \pi. \tag{29}$$

Next, the values of the separatrices p_{sep} are determined numerically using an N-th polynomial function. Specifically, this involves fixing the value of $K = K_{sep}$ at the point when the system crosses the separatrix

$$p_{sep} = \sum_{i=0}^{N} c_i \sigma^i. \tag{30}$$

It is found that the separatrices are approximated with good accuracy with a 4th order polynomial. The lower and upper separatrices are identified as p_{sep}^{low} and p_{sep}^{up}. Firstly, the integral at the denominator of Eq.28 is solved as

$$\int_{l_1} \frac{d\tilde{\bar{\mathcal{H}}}_{1:1}}{dt} dt = \int_{l_1} \frac{d\tilde{\bar{\mathcal{H}}}_{1:1}}{dp} T_L dt + \int_{l_1} \frac{d\tilde{\bar{\mathcal{H}}}_{1:1}}{dK} T_K dt = \tag{31}$$

$$= \int_{\pi}^{0} T_L d\sigma + \int_{\pi}^{0} \frac{d\tilde{\bar{\mathcal{H}}}_{1:1}}{dK} \frac{1}{d\tilde{\bar{\mathcal{H}}}_{1:1}/dp} T_K d\sigma. \tag{32}$$

The expression is evaluated at $p = p_{sep}^{up}(\sigma)$ and numerically integrated using the global adaptive quadrature method [16]. The global adaptive quadrature divides the integration domain into smaller subintervals and compute the integral over each subinterval separately. The integral is then approximated as the sum of the integrals over the subintervals. The subintervals are chosen in such a way that the error in the approximation is minimized. In a similar way, the numerator is developed.

4.2 Pendulum approximation

As for the complete model, the value of the Hamiltonian is normalized, so that $\hat{\bar{\mathcal{H}}}_{1:1} = \hat{\mathcal{H}}_{1:1} - \hat{A}$. The new Hamiltonian $\hat{\bar{\mathcal{H}}}_{1:1}$ is

$$\hat{\bar{\mathcal{H}}}_{1:1} = -\frac{1}{2} \alpha p^2 + 2\hat{A} \sin^2 \sigma. \tag{33}$$

The non-conservative contributions T_L and T_K from Eq.14 and Eq.21 are approximated as

$$T_L = \varepsilon L^2 \sim \varepsilon(L_r^2 + 2L_r p) \tag{34}$$
$$T_K = \varepsilon L K = \varepsilon(L_r K + K p), \tag{35}$$

in which the second-order term is neglected. Using the chain rule and the perturbed Hamilton's equation, the rate of change of $\hat{\bar{\mathcal{H}}}_{1:1}$ is defined as

Table 2: Initial conditions

Resonance angle	$[0, 2\pi]$
Semi-major axis	$[690, 700]$ km
Eccentricity	0.5

$$\frac{d\hat{\mathcal{H}}_{1:1}}{dt} = -\alpha p \, T_L + 4\hat{A} \sin \sigma \cos \sigma \, T_\sigma + 2\frac{dA}{dK} \sin^2 \sigma \, T_K. \tag{36}$$

Along the separatrix l_1, the Hamiltonian $\hat{\mathcal{H}}_{1:1} = 0$, so

$$p_{sep} = \pm 2\sqrt{\frac{A}{\alpha}} \sin \sigma. \tag{37}$$

Combining Eq.36 and Eq.37, the probability of capture into 1:1 GTR is

$$Pr = \frac{16 L_r \sqrt{\frac{\hat{A}}{\alpha}} - 4\frac{\partial \hat{A}}{\partial K} L_r K \frac{1}{\sqrt{\hat{A}\alpha}}}{\pi L_r^2 + 8 L_r \sqrt{\frac{\hat{A}}{\alpha}} - 2 L_r K \frac{\partial \hat{A}}{\partial K} \frac{1}{\sqrt{\hat{A}\alpha}} - \frac{\pi}{\alpha} K \frac{\partial \hat{A}}{\partial K}}. \tag{38}$$

The probability formulation is independent of the spacecraft mass and the thrust magnitude, as can be observed from the equation. By analyzing each term, the dominant terms in the probability formulation are identified. For the pendulum approximation, the probability of capture into the 1:1 GTR in the equatorial case is simplified to

$$Pr = \frac{2}{\frac{\pi}{8} \sqrt[3]{\frac{\mu}{\dot{\theta}^2 C_{22}^{3/2} R_e^3}} + 1}. \tag{39}$$

In the following sections, the probability estimation methods will be referred to as follows: the estimation using Eq.27 will be called the numerical approach, the estimation using Eq.28 will be called the semi-analytical approach, and the estimation using Eq.38 will be called the analytical approach.

5 RESULTS

This section presents the estimations obtained using the semi-analytical and analytical methods and compares them with the numerical estimations. The probability of capture is estimated for three cases based on the thrust magnitude intervals: high thrust magnitude cases with $T = [20, 90]$ mN, low thrust magnitude cases with $T = [0.2, 20]$ mN, and very low-thrust magnitude cases with $T = [0.02, 0.2]$ mN. If not specified, the initial conditions for the simulations are listed in Table 2.

5.1 Sensitivity on the thrust magnitude

The probability estimations obtained using the three approaches are compared and presented in Fig.4. For each of the three thrust magnitude intervals, the probability is estimated for 100 different thrust magnitudes, which are uniformly distributed within the given interval. For each thrust magnitude, 1000 trajectories are numerically propagated. The initial conditions of these trajectories are uniformly distributed with 100 different values for p and 10 different values for σ. The probability estimated
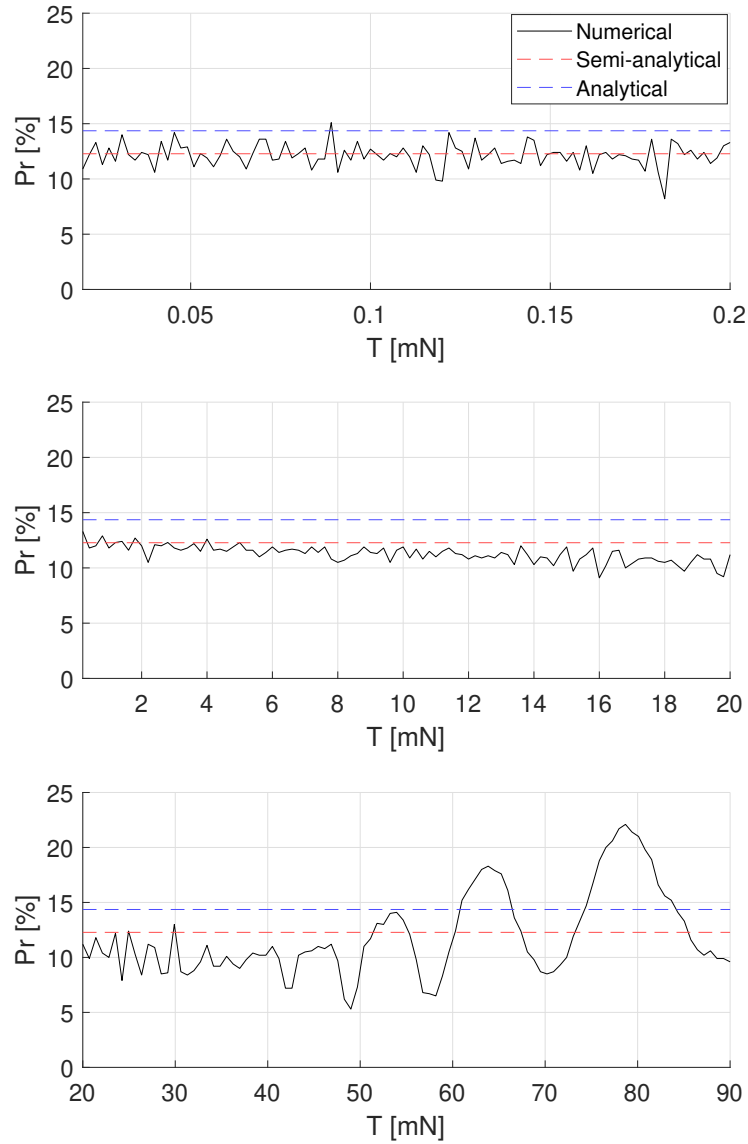
Figure 4: Probability of capture into 1:1 resonance for $e = 0.5$ and $T = [0.02, 0.2]$ mN (upper plot), $T = [0.2, 20]$ mN (middle plot) and $T = [20, 90]$ mN (lower plot). The black line represents the probability of capture estimated using numerical simulation, the red dashed line represents the probability of capture estimated using the semi-analytical approach and the blue dashed line represents the probability of capture estimated using the analytical formulation.

numerically is represented with a black line in the three plots, while the semi-analytical and analytical results are represented by red and blue dashed lines, respectively. The semi-analytical and analytical estimations of probability are found to be independent of the thrust magnitude. For the very low-thrust magnitude cases, the semi-analytical estimation is in good agreement with the average numerical estimation, while the analytical one overestimates the probability. As the thrust magnitude increases, the probability of capture decreases on average and the semi-analytical and analytical methodologies do not follow this trend. For the high thrust magnitude case, the numerically estimated probability of capture shows an oscillatory behavior, and the new estimation methodologies are not able to accurately estimate the probability of capture for these two cases. For this reason, in the last part of the paper, the thrust magnitude interval between 0.02 mN and 0.2 mN is considered.

5.2 Sensitivity on the initial eccentricity

This section analyzes the sensitivity of the probability of capture to changes of the initial eccentricity. Fig.5 shows the probability of capture for various eccentricity values. The average value of the numerically estimated probability of capture remains constant for all eccentricity values. For small eccentricities, the probability of capture estimated with the semi-analytical and analytical methodologies matches with each other. However, as the eccentricity increases, the semi-analytical estimation approaches the numerical estimation. These observations are summarized in Fig.6. For low eccentricity values, the numerical estimation remains almost constant at approximately 12.7%, whereas it increases to around 13.8% as the eccentricity increases. The analytical estimation (blue line) gives an almost constant value of about 14.36%, serving as an upper bound for the mean probability of capture. The semi-analytical estimation correctly estimates the probability of capture for high eccentricity cases and converges to the analytical estimation as the eccentricity decreases. This is due to the fact that the phase space of the complete model closely resembles that of the Hamiltonian's pendulum approximation, as illustrated in Fig.7.

6 CONCLUSIONS

The purpose of the current study is to introduce a semi-analytical approach to estimate the probability of capture into 1:1 GTR of Dawn around Vesta. The proposed two-degree-of-freedom Hamiltonian model includes the effects of the spherical harmonic approximation of the gravity field of the asteroid up to the second order and degree. Additionally, the effect of the low-thrust is taken into account by modifying Hamilton's equations. The general formulation of the probability of capture into resonance is presented and adapted for the case under consideration. An approximation of the Hamiltonian model is developed by expanding the function around the location of the resonance, which leads to an analytical formulation of the probability of capture. The results from the semi-analytical and analytical methodologies are compared with the ones obtained numerically. Then, the sensitivity of the probability with respect to the thrust magnitude and eccentricity is analyzed. It is found that the methodologies are suitable for very low thrust magnitudes and high eccentricity. For low eccentricity values the analytical and semi-analytical methodologies provide an upper bound value for the probability of capture. In the future, additional investigations are recommended to adapt the methodologies for low eccentricity cases and generalize the methodologies for other GTR, such as the 2:3 GTR which is one of the main resonances around Vesta.

REFERENCES

[1] P. Tricarico and M. Sykes, "The dynamical environment of dawn at vesta," *Planetary and Space Science*, vol. 58, pp. 1516–1525, 2010. DOI: `10.1016/j.pss.2010.07.017`.
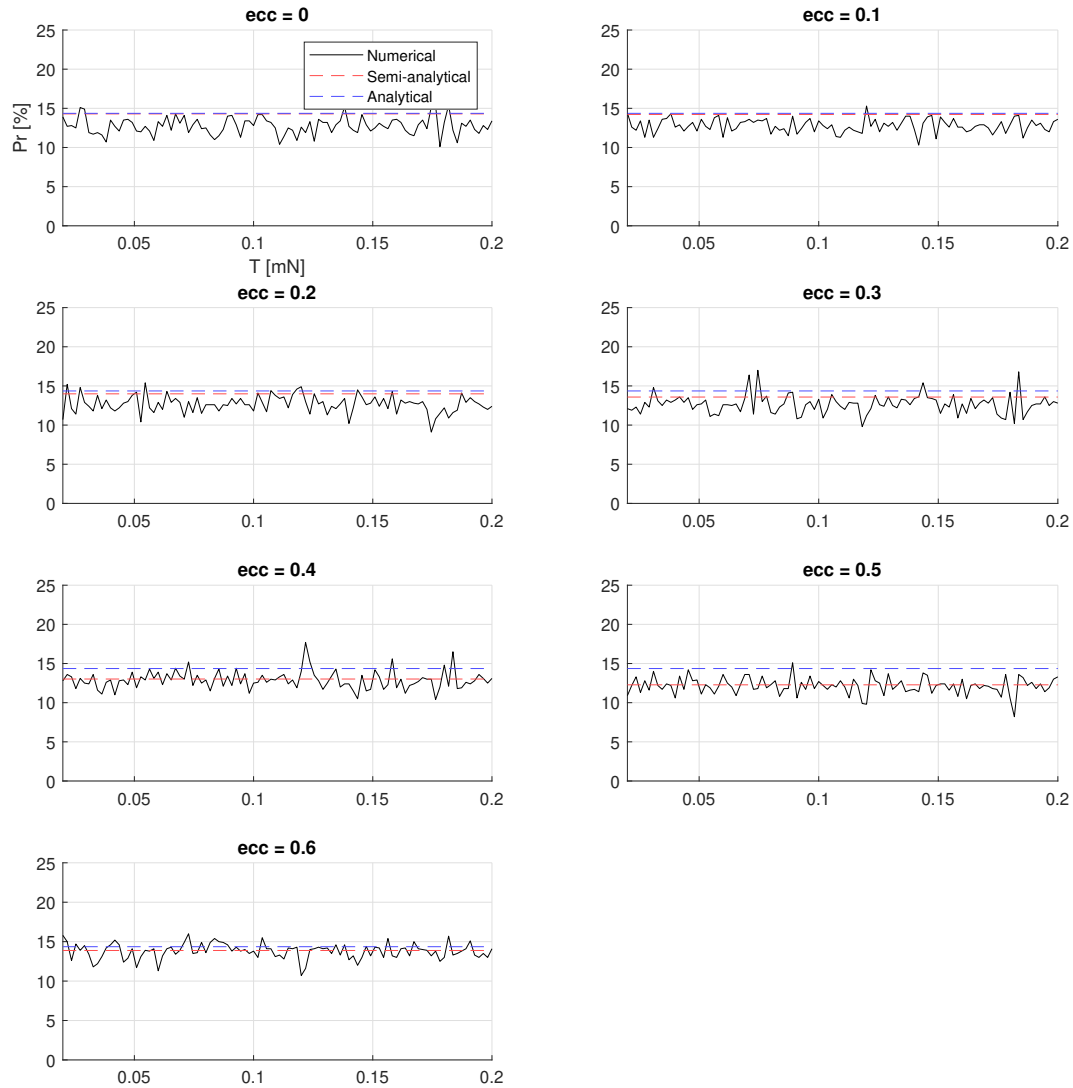
Figure 5: Probability of capture into 1:1 resonance for $T = [0.02, 0.2]$ mN and for $e = [0, 0.6]$. The black line represents the probability of capture estimated using numerical simulation, the red dashed line represents the probability of capture estimated using the semi-analytical approach and the blue dashed line represents the probability of capture estimated using the analytical formulation.
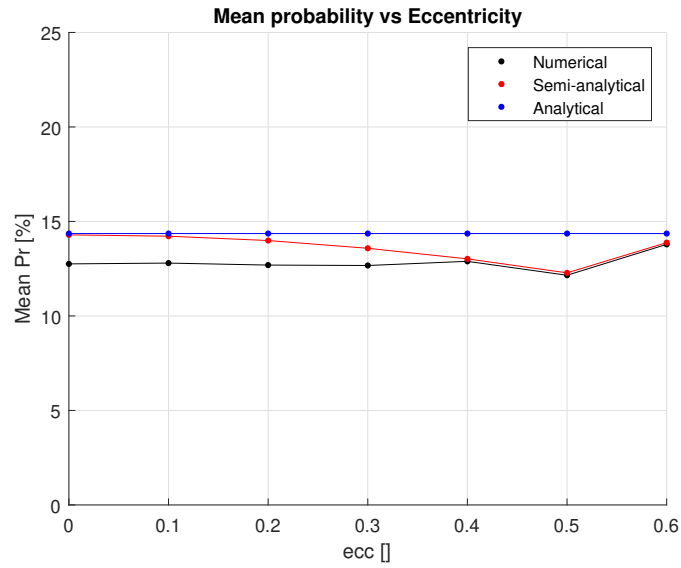
Figure 6: Average probability of capture into 1:1 GTR for $T = [0.02, 0.2]$ mN and for $e = [0, 0.6]$. The black line represents the probability of capture estimated using numerical simulation, the red dashed line represents the probability of capture estimated using the semi-analytical approach and the blue dashed line represents the probability of capture estimated using the analytical formulation.
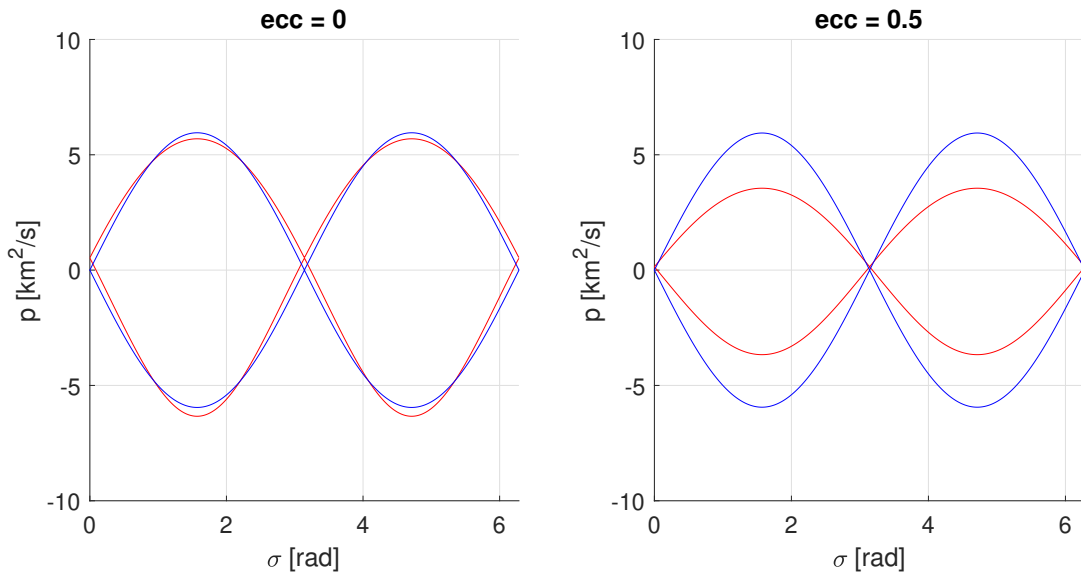

Figure 7: Phase space comparison between complete (red lines) and approximated (blue lines) Hamiltonians for $e = 0$ (left plot) and $e = 0.5$ (right plot).

[2]   A. Celletti and C. Gales, "On the dynamics of space debris: 1:1 and 2:1 resonances," *J Nonlinear Sci*, vol. 24, pp. 1231–1262, 2014. DOI: `10.1007/s00332-014-9217-6`.

[3]   A. Celletti, C. Gales, and C. Lhotka, "Resonances in the earth's space environment," *Communications in Nonlinear Science and Numerical Simulation*, vol. 84, pp. 105–185, 2020. DOI: `10.1016/j.cnsns.2020.105185`.

[4]   K. Nishiyama, S. Hosoda, K. Ueno, R. Tsukizaki, and H. Kuninaka, "Development and testing of the hayabusa 2 ion engine system," *The Japan Society for Aeronautical and Space Sciences*, vol. 14, pp. 131–140, 2016. DOI: `10.2322/tastj.14.Pb_131`.

[5]   N. Wallace, O. Sutherland, J. Bolter, *et al.*, "Bepicolombo - solar electric propulsion system operations for the transit to mercury," 2019.

[6]   D. Morante, M. Sanjurjo Rivo, and M. Soler, "A survey on low-thrust trajectory optimization approaches," *Aerospace*, vol. 88, 2021. DOI: `10.3390/aerospace8030088`.

[7]   D. Scheeres, "Orbital mechanics about small bodies," *Acta Astronautica*, vol. 72, pp. 1–14, 2012. DOI: `10.1016/j.actaastro.2011.10.021`.

[8]   J. Feng, R. Noomen, and X. Hou, "1:1 ground-track resonance in a uniformly rotating 4th degree and order gravitational field," *Celestial mechanics and dynamical astronomy*, vol. 127, pp. 67–93, 2017. DOI: `10.1007/s10569-016-9717-9`.

[9]   O. Montenbruck and G. Eberhard, *Satellite Orbits - Models, Methods and Applications*. DOI: `10.1115/1.1451162`.

[10]   W. Kaula, *Theory of Satellite Geodesy: Applications of Satellites to Geodesy*. 1966.

[11]   D. Scheeres, "The effect of c22 on orbit energy and angular momentum," *Celestial Mechanics and Dynamical Astronomy*, vol. 73, pp. 339–348, 1999. DOI: `10.1023/A:1008384021964`.

[12]   C. Lhotka, A. Celletti, and C. Gales, "Poynting–robertson drag and solar wind in the space debris problem," *Monthly Notices of the Royal Astronomical Society*, vol. 460, pp. 802–815, 2016. DOI: `10.1093/mnras/stw927`.

[13]   D. Okhotsimskii and Y. Sikharulidze, *Fundamentals of Space Flight Mechanics*. 1990.

[14]   A. Neishtadt, "Averaging method for systems with separatrix crossing," *Nonlinearity*, vol. 30, 2017. DOI: `10.1088/1361-6544/aa712f`.

[15]   A. Neishtadt, "Passage through a separatrix in a resonance problem with a slowly-varying parameter," *Journal of Applied Mathematics and Mechanics*, vol. 4, 1975. DOI: `10.1016/0021-8928(75)90060-X`.

[16]   L. Shampine, "Vectorized adaptive quadrature in matlab," *Journal of Computational and Applied Mathematics*, vol. 211, pp. 131–140, 2008.